International Journal of Multiphase Flow 103 (2018) 30–42

Contents lists available at ScienceDirect

International Journal of Multiphase Flow

journal homepage: www.elsevier.com/locate/ijmulflow

Control of minimum film-boiling quench temperature of small spheres with micro-structured surface☆

Kang Jun-young[a], Lee Gi Cheol[b], Massoud Kaviany[c,d], Park Hyun Sun[d], Kiyofumi Moriyama[d], Kim Moo Hwan[d,*]

[a] Thermal-Hydraulic Safety Research Division, KAERI, Daejoen 34057, South Korea
[b] Department of Mechanical Engineering, POSTECH, Pohang 790-784, South Korea
[c] Department of Mechanical Engineering, University of Michigan, Ann Arbor, MI 48109, USA
[d] Division of Advanced Nuclear Engineering, POSTECH, Pohang 790-784, South Korea

ARTICLE INFO

Article history:
Received 10 March 2017
Revised 22 January 2018
Accepted 24 January 2018
Available online 19 February 2018

ABSTRACT

The control of minimum film-boiling quench temperature, T_{MFB} is investigated in water quenching experiments with several micro-structured surfaces on small spheres (diameters 10 and 15 mm) under saturation temperature T_{sat} and 1 atm. The results show increase in T_{MFB} and is related to the temperature drop across the micro-structures, and affected by its effective thermal conductivity $\langle k \rangle$, height L, and base diameter D, based on the fin theory. The local temperature drop of surface microstructure depends on the *hybrid Biot number*, $Bi_h = hL^2/(\langle k \rangle D)$, where h is the heat transfer coefficient. The liquid–solid contact depends on this microstructure-tip temperature, and a model for T_{MFB} with synthetic surface microstructure is proposed and compared with the experimental results. The theoretical limit of maximum T_{MFB} (under saturated water at 1 atm) for surface micro-structured small sphere is reached when $\mathrm{Bi_h}$ is beyond 10^2.

1. Introduction

In film boiling, high wall temperature T_w hinders a liquid–solid contact, and the heat is mainly transferred by conduction across the vapor film and radiation towards ambient temperature. Minimum film-boiling quench temperature T_{MFB} is the minimum temperature required to sustain a stable vapor film in film boiling, and marks transition from film to transition boiling regimes during quenching. The heat transfer coefficient h undergoes a large change during this transition (h $\langle 5 \times 10^2$ and$\rangle$ 5×10^2 to 10^3 W/(m^2-K) for the film and transition boiling regimes, respectively). So, the control (i.e., increase) of T_{MFB} significantly impacts the cooling rate during quenching (Bromley, 1948). Therefore, comprehensive study in T_{MFB} is essential for development of high-temperature cooling systems such as the emergency core-cooling systems of nuclear power plants, cryogenics, and metallurgic systems (Bang and Jeong, 2011).

Over the decades, quenching studies have focused on an increase in T_{MFB}, by micro-texturing the heat transfer surface (Shoji et al., 1990; Sinha, 2003; Kim et al., 2009; Lee et al., 2016; Kang et al., 2016, 2017; Kozlov and Keßler, 2016). In film boiling, liquid–solid contact, intermittently induced by surface microstructures, causes an increase in T_{MFB} (Bradfield, 1966). However, questions remain regarding the relationship between the liquid–solid contact and characteristics of surface micro-structures. Recently, we reported an increase in T_{MFB} using micro-structured CuO surfaces and explained it by the fin theory to predict the fin temperature distribution and through that the liquid–solid contact (Kang et al., 2017). Major parameters in surface micro-structures that influence the liquid–solid contact are the effective thermal conductivity $\langle k \rangle$ and characteristic length L^2/D of micro-structures, where L and D are the fin height and fin base diameter, respectively.

Herein, we expand our knowledge about T_{MFB} on a micro-structured surface. We prepared several surface micro-structures on metal spheres (diameter d_{sphere} of 10 and 15 mm, using brass and stainless steel), and conducted a water quenching experiment under saturation temperature T_{sat} and 1 atm. The objectives of this study are (i) to observe the T_{MFB} behavior depending on characteristics of surface micro-structures, (ii) to develop a model for predicting T_{MFB} on such surfaces, and (iii) to suggest the theoretical limit of T_{MFB} increase by surface micro-structures.

☆ Dr. Jun-young Kang is applying as the post-doctoral researcher in KAERI, and this work is based on his doctoral dissertation (Rep. of Korea, POSTECH, 2017).

* Corresponding author.
E-mail address: mhkim@postech.ac.kr (K. Moo Hwan).

https://doi.org/10.1016/j.ijmultiphaseflow.2018.01.022
0301-9322/

Table 1
Summary of proposed model for minimum film-boiling quench temperature.

Equation	Number	Reference
$T_{\mathrm{MFB}} = T_{sat} + 0.127\frac{\rho_v h_{lv}}{k_v}[\frac{g(\rho_l-\rho_v)}{\rho_l+\rho_v}]^{2/3}[\frac{\sigma_{lv}}{g(\rho_l-\rho_v)}]^{1/2}[\frac{\mu_v}{g(\rho_l-\rho_v)}]^{1/3}$	(1)	Taylor–Helmholtz hydrodynamic instability (Berenson 1961)
$T_{MFB} = T_{MFB,B} + 0.42(T_{MFB,B} - T_l) \times \{[\frac{(\rho C_p k)_l}{(\rho C_p k)_s}]^{0.5} h_{lv}/[C_{p,s}(T_{MFB,B} - T_{sat})]\}^{0.6}$	(2)	Taylor–Helmholtz hydrodynamic instability with liquid–solid contact (Henry 1974)[a]
$T_{\mathrm{MFB}} = (\frac{27}{32})T_{cr}$	(3)	Thermodynamic superheat limit of liquid (Spiegler et al., 1963)
$T_{\mathrm{MFB}} = \frac{(\frac{27}{32})T_{cr}\{1-\exp[-0.52(\frac{10^4(\rho/n_0)^{4/3}}{\sigma_{lv}})^{1/3}]\}-T_l}{\exp[0.00175(\rho C_p k)_s^{-1}]erfc(0.042(\rho C_p k)_s^{-1/2})} + T_l$	(4)	Effect of surface thermal properties and surface tension of matters (Baumeister and Simon 1973)
$T_{\mathrm{MFB}} = T_{sat} + 101 + 8\Delta T_{sub}$	(5)	Effect of liquid subcooling (Dhir and Purohit 1978)
$T_{\mathrm{MFB}} = T_{sat} + 0.6[(\frac{27}{32})T_{cr} - T_{sat}] + \frac{(\frac{k_v}{k_l})\mathrm{Nu}_l\Delta T_{sub}}{(\frac{d}{\delta_{v,min}}+\mathrm{Nu}_{rad})}$	(6)	Effect of liquid subcooling (Kondo et al., 1995)
$T_{\mathrm{MFB}} = T_{sat} + 0.29(T_{MFB,B} - T_{sat})(1 - 0.295{x_e}^{2.45})(1 + 0.279G^{0.49})$	(7)	Effect of forced convection (Iloeje et al. 1975)
$T_{\mathrm{MFB}} = 0.92T_{cr}\{1 - 0.26\exp[\frac{-20(\frac{P}{P_{cr}})}{1+\frac{1700}{P_{cr}}}]\}(1 + (\frac{k_l\rho_l C_{p,l}}{k_s\rho_s C_{p,s}})^{1/2}) - T_{sat}(\frac{k_l\rho_l C_{p,l}}{k_s\rho_s C_{p,s}})^{1/2}$	(8)	Effect of system pressure (Sakurai et al. 1990)
$T_{\mathrm{MFB}} = [(1 - \cos(C.A)(\frac{\sigma_{lv}V_{m,l}}{B})]^{\frac{a_1-a_2}{a_2}} + T$	(9)	Effect of surface wetting (Olek et al. 1988)[b]
$T_{\mathrm{MFB}} = \{[1 + (\frac{k_l\rho_l C_{p,l}}{k_s\rho_s C_{p,s}})^{1/2}]\frac{Q_a}{R_g}\frac{1}{\ln(9\frac{(2\pi MR_gT)^{1/2}\Gamma_0}{N_A P t_0})}\} - (\frac{k_l\rho_l C_{p,l}}{k_s\rho_s C_{p,s}})^{1/2}T_l$	(10)	Effect of surface wetting (Segev and Bankoff 1980)[c]

Note: The nomenclatures in Table 1 are summarized as follow; ρ, k, g, μ, h_{lv}, σ_{lv}, C_{p}, T_{cr}, P_{cr}, ΔT_{sub}, d, $\delta_{\mathrm{v,min}}$, Nu, $\mathrm{Nu}_{\mathrm{rad}}$, x_{e}, G, n_0, T, T_{l}, and P are the density, thermal conductivity, gravitational acceleration, viscosity, latent heat of vaporization, surface tension, specific heat, critical temperature, critical pressure, liquid subcooling, diameter, minimum vapor film thickness, Nusselt number, radiation Nusselt number, exit quality, mass flux, atomic number, temperature, liquid temperature and pressure, respectively. The physical properties with subscripts '*v*', '*l*", and '*s*' denote those of vapor, liquid and solid, respectively.

[a] $T_{\mathrm{MFB,B}}$ denotes the minimum film-boiling temperature suggested by Berenson (1961).

[b] T_{MFB} is defined as the surface temperature corresponding to zero contact angle, and can be obtained by curve fitting to experimental results. The C.A., V_{m}, and B (or, a_1, and a_2) are the contact angle, molecular volume, and fitting constant, respectively.

[c] T_{MFB} is defined as the surface temperature at highly adsorbed state: $\varepsilon = \Gamma/\Gamma_0 = 0.9$ where ε, Γ and Γ_0 are the dimensionless occupancy, the number of adsorbed molecules per unit area, and, the number of adsorbed molecules per unit area which form a monolayer, respectively. The Q_{a}, M, N_{A}, R_{g}, and t_0 are the heat of adsorption, molecular weight, *Avogadro's* number, gas constant, and residence time of molecule in adsorbed state, respectively.

2. Background

The T_{MFB} is explained by *hydrodynamic* or *thermodynamic* models (Bernardin, 1999) (Table 1). The hydrodynamic model is based on the minimum heat flux q''_{min} predicted by a *Taylor-type* instability (Eq. (1)) (Berenson, 1961). The thermodynamic model (Eq. (3)) is derived from the foam limit of a stable vapor film, determined by the van der Waals equation (Spiegler et al., 1963). A number of studies have reported the thermo-physical properties of the heat transfer surface with the surface tension of liquid-vapor and liquid–solid (Eqs. (2), (4)) (Henry, 1974; Baumeister and Simon, 1973), liquid subcooling (Eqs. (5), (6)) (Dhir and Purohit, 1978; Kondo et al., 1995), forced convection (Eq. (7)) (Iloeje et al., 1975), system pressure (Eq. (8)) (Sakurai et al., 1990), and surface wetting (Eqs. (9), (10)) (Olek et al., 1988; Segev and Bankoff, 1980). However, few studies have addressed the influence of surface micro-structures on T_{MFB}.

The increase in T_{MFB} by the surface micro-structures can be explained by the change in liquid–solid contact dynamics. The main variables of liquid–solid contact are the contact duration t_c, contact frequency f_c, contact area A_c, and wall temperature T_{w}. Previously published researches concerning the liquid–solid contact have not focused on the effect of surface micro-structures (Yao and Henry, 1978; Lee et al., 1982, 1985; Dhuga and Winterton, 1985; Neti et al., 1986; Chang and Witte, 1990; Kikuchi et al., 1992) (Table 2); instead, these researches mainly studied t_c, f_c, and A_c changes according to T_{w}. T_{w}, in particular, plays a crucial role in liquid–solid contact during quenching, because it is related to the superheat limit of the liquid at the liquid–solid contact site. It is well known that T_{w} causing liquid–solid contact is represented by the homogeneous nucleation temperature of the liquid T_{hn} (Carey, 1992).

The surface micro-structure is characterized in simplified terms by $\langle k\rangle$, L, and D. Earlier studies focused on only L, because we believe that micro-structures solely touch the liquid–vapor interface causing destabilization of vapor film in film boiling. A representative example is the study of a single *Leidenfrost drop* reported by Kim et al., (2011); the role of micro-structures is to trigger liquid–solid contact during film boiling. However, we should recognize that the liquid–solid contact is not only affected by L, and, is but also combined with other micro-structure parameters such as $\langle k\rangle$ and D.

This study started from a question about the relationship between the characteristics of surface micro-structures and liquid–solid contact. We expect that L, $\langle k\rangle$, and D together impact the change in T_{w} at a local spot. In contrast to smooth surfaces, a local cool-down spot can exist at microstructure-tip on surfaces, which leads to liquid–solid contact in film boiling during quenching, causing an increase in T_{MFB}. This expectation is in agreement with known quenching studies concerning T_{MFB} increase on the heat transfer surfaces coated with insulating materials (Moreaux et al., 1975; Kikuchi et al., 1985).

3. Material and method

3.1. Quench appratus and test sample

The apparatus, sample, and procedure of the quenching experiment have been developed to our previous quenching studies, and a detailed demonstration is available in several references (Kang et al., 2016, 2017, 2018a,b,c). The quenching apparatus has four components, namely, the radiation furnace, quench pool, transport device, and data acquisition system. Water quenching experiment was conducted under saturation temperature T_{sat} and 1 atm, and the initial quench temperature T_{initial} is 600 °C. When the quench sphere is heated up to T_{initial} by a radiation furnace, the transport device rapidly delivers the sphere into the quench pool containing the distilled water. The temperature of the furnace and quench pool was controlled by the P.I.D. system and its deviation was below ± 5 °C. In all quench tests, the water coolant was de-gassed. The dynamics of the liquid-vapor interface in film boiling during

Table 2
Physical parameters of liquid–solid contact.

Condition	Contact area A_c [m^2]	Contact duration t_c [ms]	Contact frequency f_c [Hz]	Reference
√ Steady-state experiment √ SUS or Copper coated by Cr or Au layer √ Ethanol or Water √ 1 atm and T_{sat} √ Electrical conductance method	Theoretical area fraction, $A_c^* = A_c/(\lambda_D)^2$ $A_c{}^* = 10$ ($T_{int} = 150$ °C, Ethanol) $A_c^* = 0.1(T_{int} = 220°C$, Water)	$t_c = 100$ ($T_{int} = 150$ °C, Ethanol) $t_c = 1{\sim}10$ ($T_{int} = 220$ °C, Water)	N/A**	Yao and Henry (1978)
√ Transient experiment √ Copper coated by Ni layer √ Water √ 1 atm and T_{sat} √ Micro-thermocouple method	N/A	Time fraction, $t_c^* = t_c/(t_{c,r} + t_c)$ $t_c = 0.5{\sim}5$ (T_w ~236 °C) $t_c^* = 0.1{\sim}0.15$ (T_w ~236 °C) $t_c = 1{\sim}100$ (T_w ~160 °C) $t_c^* = 0.2{\sim}0.4$ (T_w ~160 °C)	N/A	Lee et al. (1982)
√ Transient experiment √ Copper coated by Al layer √ Water √ 1 atm and T_{sat} √ Micro-thermocouple Method	N/A	$t_c = 0.5{\sim}32$ (ΔT_{sat}: 42.5 °C~114.5 °C) $t_c^* = 0.5$ (T_w ~30 °C) $t_c^* = 0.003$ (T_w ~200 °C)	$f_c = 5$ ($\Delta T_{sat} > 180$ °C) $f_c = 50$ (ΔT_{sat}: 100 °C~180 °C) $f_c = 30$ ($\Delta T_{sat} < 100$ °C)	Lee et al. (1985)
√ Transient experiment √ Anodized aluminum √ Water or Methanol √ 1 atm and T_{sat} √ Impedance measurement	Measured area fraction, A_c** A_c ** = 0.2 (ΔT_{sat}~180 °C, Water) A_c ** = 0.02 (ΔT_{sat}~260 °C, Water) A_c ** = 0.2 (ΔT_{sat}~60 °C, Methanol) A_c ** = 0.015 (ΔT_{sat}~70 °C, Methanol)	N/A	N/A	Dhuga and Winterto-n (1985)
√ Transient experiment √ Vycor glass √ Water √ 1 atm and T_{sat} √ Fiber optic measurement	N/A	$t_c^* = 0.001{\sim}0.0015$ (ΔT_{sat} ~750 °C) $t_c^* = 0.01{\sim}0.1$ (ΔT_{sat}: 610 °C~650 °C)	N/A	Neti et al. (1986)
√ Steady-state experiment √ Hasteloy-C √ Freon-11 √ 1 atm and T_{sat} √ Micro thermocouple method	N/A	$t_c^* = 0.0035$ (ΔT_{sat} ~180 °C) $t_c^* = 0.02$ (ΔT_{sat} ~160 °C) $t_c^* = 0.08$ (ΔT_{sat} ~120 °C)	$f_c = 0.03$ (ΔT_{sat} ~180 °C) $f_c = 0.4$ (ΔT_{sat} ~160 °C) $f_c = 1$ (ΔT_{sat} ~120 °C)	Chang and Witte (1990)
√ Transient experiment √ Silver sphere √ Water √ 1 atm and T_{sat} √ Impedance measurement	N/A	N/A	$f_c = 2.2$ (T_w: 600 °C~650 °C) $f_c = 2.6$(T_w: 550 °C~600 °C) $f_c = 2.7$ (T_w: 500 °C~550 °C) $f_c = 3.1$ (T_w: 450 °C~550 °C)	Kikuchi et al. (1992)

Note: The nomenclatures in Table 2 are summarized as follow; the Tint, λD, t_c,r, and ΔT_{sat} are the interface temperature between two semi-infinite mediums (Henry 1974), the most dangerous wavelength, the residual time before/after the contact duration, and wall superheat, respectively. The N/A indicates not-available. A* and A** indicate the area fraction based on a theoretic and experimental, respectively.

Table 3
Test matrix in quench experiments.

I.D.	Substrate material	Structure material	Diameter of sphere, d_{sphere} [mm]	ENP treatment	Annealing
$RS_{SUS316L}$	SUS316L	–	10	X	O
$MS_{SUS316L}$	SUS316L	SUS316L	10	X	O
RS_{Brass}	Brass	–	10 and 15	O	O
MS_{Brass}	Brass	Brass	10 and 15	O	O
MS_{CuO}	Brass	CuO	15	X	O
$MNS_{Brass/CuO}$	Brass	Brass & CuO	15	X	O
NS_{CuO}	Brass	CuO	15	X	O
RS_{Zr}	Zr-702	–	15	X	O
MS_{ZrO2}	Zr-702	ZrO_2	15	X	O

quenching was also recorded using a high-speed camera (Vision research, Phantom Miro).

We selected quench spheres with different sizes (diameter d_{sphere} of 10 and 15 mm) and different materials (Brass and stainless steel). The test matrix is summarized in Table 3. Test spheres were purchased by Kopeco Co., Ltd. The temperature during quenching was obtained by K-type thermocouple inserted into the center of the quench sphere (Omega; Inconel-sheath; 500 µm). The contact resistance at the junction of the sphere thermocouple was minimized using thermal grease. The supporting guide (1/16″, SUS316L) was installed in a quench sphere to hold the test sample, to transport the device, and to prevent the thermal damage of thermocouple in a quenching environment. We checked that the error in the thermocouple used in this study was below ± 1 °C, by calibrating it at Korean Measurement Technical Laboratory Co. Ltd.

Due to the small sphere Biot number [$Bi_{sphere} = hL_c/k = hV/(Ak) = 0.02$ for SUS316 ($d_{sphere} = 10$ mm), 0.006 for brass ($d_{sphere} = 15$ mm)], the lumped-capacitance approximation is used for T_{MFB} (Cengel, 2003), where L_c, V, and A are the characteristic length, volume and area of the sphere, respectively. This indicates the temperature distribution within the sphere is negligible in the film boiling regime. The heat transfer coefficient h is evaluated by the temperature variation dT/dt during the film boiling [$h = \rho Cp(V/A)(dT/dt)/(T_{(t)} - T_{sat})$, where ρ and C_p are the density and specific heat of sphere]. The error estimate of h is below 5% when Bi_{sphere} is below 0.1. By converting the quench curve to the

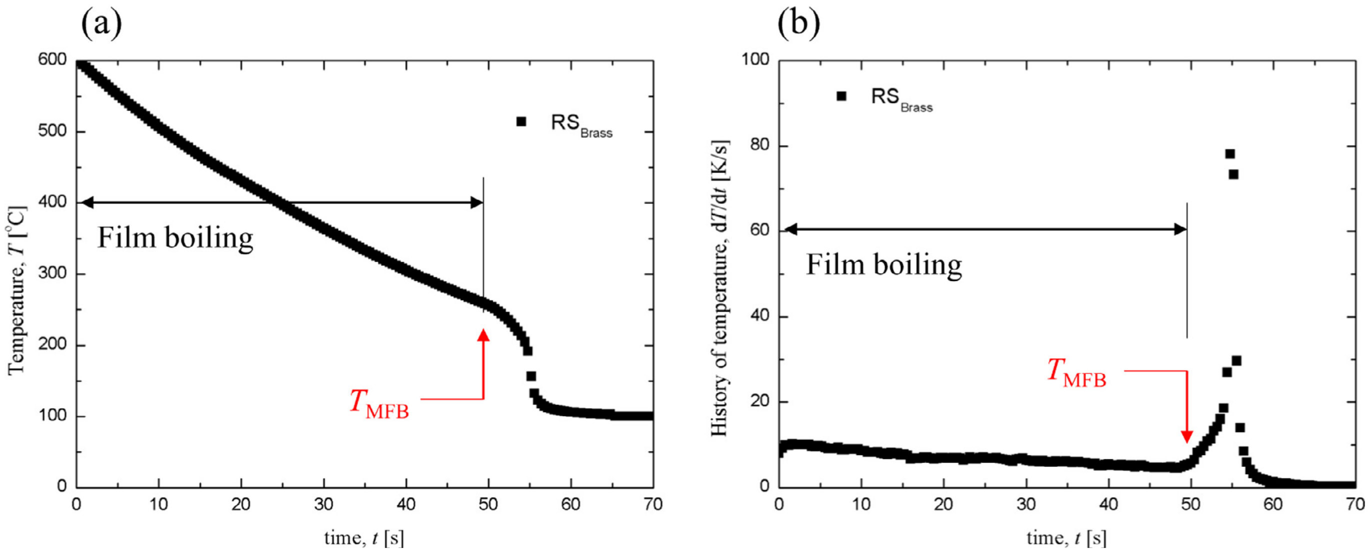

Fig. 1. Determination of minimum film-boiling quench temperature T_{MFB}: (a) quench curve, and (b) cooling rate curve.

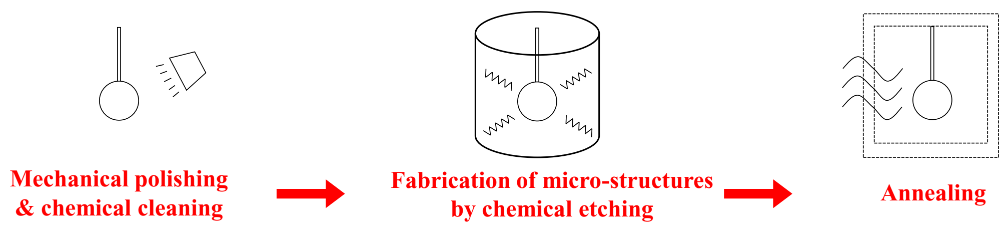

Fig. 2. Fabrication process of micro-structured surface.

cooling rate curve (Fig. 1a), T_{MFB} is calculated and corresponds to the minimum dT/dt (Fig. 1b).

3.2. Surface preparation

Prior to fabrication, all surfaces of the quench spheres were polished using sandpaper (2000-grit, Daesung) and chemically cleaned by acetone, ethanol, and distilled water, sequentially. The smooth surface is referred to as a reference surface (RS). We prepared three micro-structured surfaces (MS) to investigate the impact in T_{MFB} depending on the micro-structure characteristics: micro-structured surface of SUS316L ($MS_{SUS316L}$), micro-structured surface of brass (MS_{Brass}), and hierarchical micro- and nano-structured surface ($MNS_{Brass/CuO}$). In this study, the fabrication in surface micro-structures is based on the chemical etching method and detailed recipe depends on the test materials (Fig. 2), following the below description.

- In case of $MS_{SUS316L}$, SUS316L ($d_{sphere} = 10$ mm) sphere was etched in 0.9 wt% nitric acid (HNO_3) with 2.7 wt% hydrochloric acid (HCl) as an electrolyte with a constant electrical potential $\Delta V = 18$ V for a reaction time, $t_r = 30$ s (Lee and Kim, 2015).
- In case of MS_{Brass}, the brass ($d_{sphere} = 10$ and 15 mm) sphere was etched by an acid solution [8 M nitric acid (HNO_3) with 1.2 M cetyl trimethylammonium (cTAB)] under ultra-sonication condition ($t_r = 1800$ s) (Pan et al., 2010).
- $MNS_{Brass/CuO}$ ($d_{sphere} = 15$ mm) was prepared by the fabrication method in MS_{Brass} with adding the CuO nanostructure-coating (Pan et al., 2010; Xiao et al., 2011). This treatment facilitates the fabrication of hierarchical surface structures on a brass sphere: CuO nano-structures on micro-structured brass.

In particular, RS_{Brass} and MS_{Brass} were treated using electroless nickel plating (ENP) to prevent additional surface oxidation under the quenching conditions (Tian et al., 2012). The thickness of the nickel layer was thin enough to ignore changes to the surface micro-structures (e.g., L and D) during the ENP process; note that k_{nickel} ~90 W/(m·K) is similar to that of brass (k_{brass} ~10^2 W/(m·K)). All surfaces underwent a heat-treatment process under 250 °C for 1 h, followed by 500 °C for 1 h before the quenching experiment to eliminate the residual chemical elements by the fabrication process.

We recently reported the T_{MFB} results using quenching experiment with small spheres and evaluated the characteristics of the micro-structured CuO surface (MS_{CuO}), nano-structured CuO surface (NS_{CuO}) (Kang et al., 2017) and micro-structured ZrO_2 surface (MS_{ZrO2}) (Kang et al., 2018c), respectively. For analyzing the relation between T_{MFB} and surface micro-structures, we provide our recent results from the surface characteristics to the quench data as support data.

3.3. Surface characterization

The surface morphology was observed using field-emission scanning electron microscopy (FE-SEM) (Fig. 3). All reference surfaces (e.g., RS_{Brass}, $RS_{SUS316L}$ and RS_{ZrO2}) seem to be smooth and slightly scratched, caused by the sand-paper surface finish, and the surface micro-structures were regularly distributed around each micro-structured surface (e.g., MS_{Brass}, $MS_{SUS316L}$, MS_{ZrO2}, and MS_{CuO}), NS_{CuO} and $MNS_{Brass/CuO}$. The roughness (or, fin) height L, and roughness diameter D of surface and the contact angle (C.A.) were measured using FE-SEM with the surface profiler (KLA Tencor, Alphastep-IQ) and contact angle measurement system (Femtofab, Smart-Drop), respectively. Its average values were summarized in Table 4. In particular, the C.A. strongly related to surface morphology was nearly identical for MS_{Brass} and $MS_{SUS316L}$ (C.A.~55°). In addition, the contact angle for MS_{CuO}, $MNS_{Brass/CuO}$, NS_{CuO}, MS_{ZrO2}

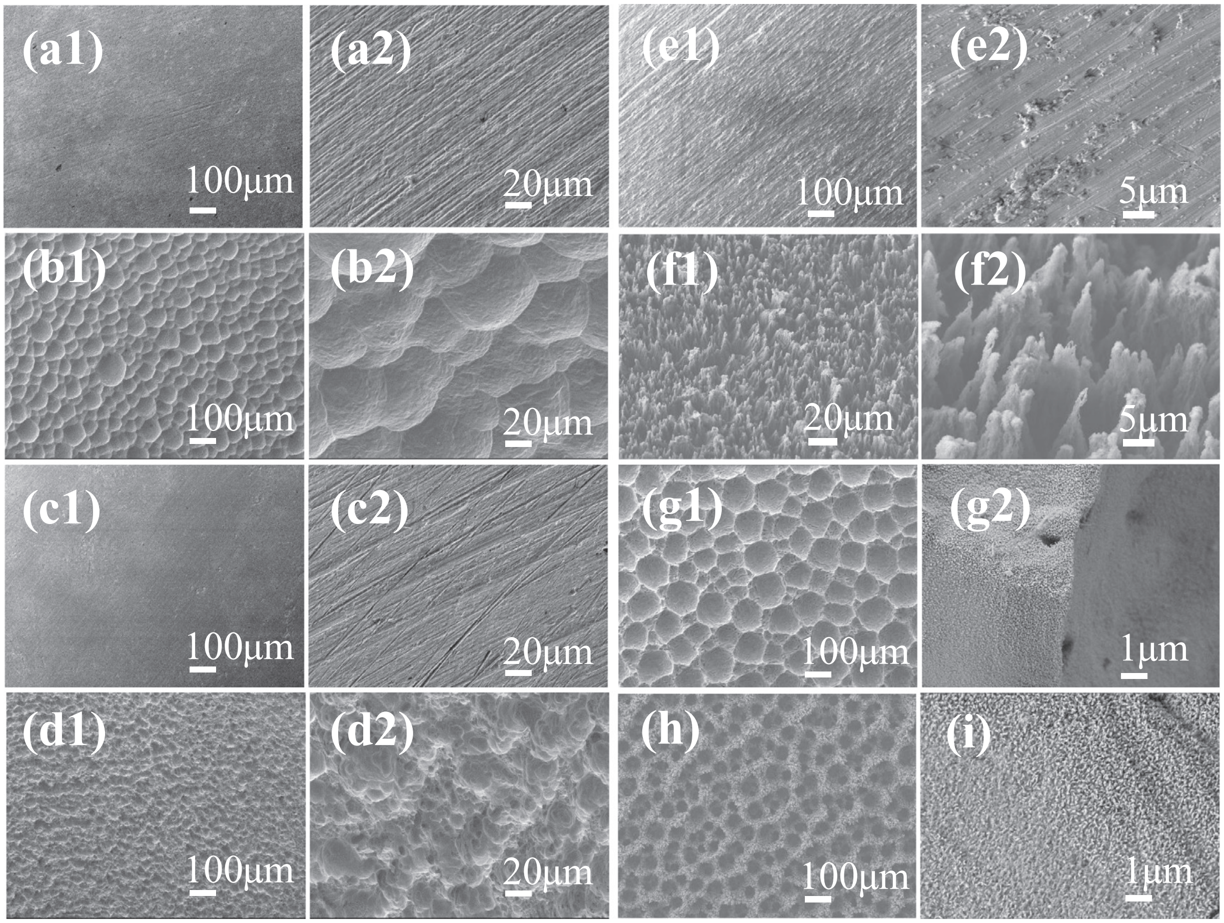

Fig. 3. Surface morphology for the reference surface (RS) and micro-structured surface (MS) for each material: (a1,a2) RS_{Brass}, (b1,b2) MS_{Brass}, (c1,c2) $RS_{SUS316L}$, (d1,d2) $MS_{SUS316L}$, (e1,e2) RS_{Zr}, (f1,f2) MS_{ZrO2}, (g1,g2) $MNS_{Brass/CuO}$, (h) MS_{CuO} and (i) NS_{CuO}.

Table 4
Surface parameters for different quench spheres.

I.D.	Contact angle, C.A, [°]	Height of Structures *L*, [μm]	Base diameter of Structures *D*, [μm]	Structure material	Structures shape	Structure scale	Porous characteristics of micro-structure
$RS_{SUS316L}$	50 ± 6	~0.1	~0.1	–	–	–	X
RS_{Brass}	55 ± 3	~0.1	~0.1	–	–	–	X
$MS_{SUS316L}$	56 ± 4	7 ± 1	2 ± 1	SUS316L	Conical	Micro	X
MS_{Brass}	53 ± 1	11 ± 1	25 ± 3	Brass	Conical	Micro	X
$MNS_{Brass/CuO}$	~0	10 ± 2	25 ± 3	Brass & CuO	Conical	Micro/nano	X
MS_{CuO}	~0	100 ± 5	20 ± 5	CuO	Conical	Micro	O
NS_{CuO}	< 10	~0.1	~0.1	CuO	Conical	Nano	X
RS_{Zr}	64 ± 4	~0.1	~0.1	–	–	–	X
MS_{ZrO2}	~0	8 ± 3	~5	ZrO_2	Conical	Micro	O

exhibited a super-hydrophilicity (C.A.~0°). Therefore, we are able to evaluate the influence of sub-parameters in surface microstructures ($<k>$, *L*, and *D*) at T_{MFB}, except for the contact angle, separately.

4. Results

All T_{MFB} results at the quenching experiment were obtained by the three repeatability and three reproducibility tests, and average deviations of T_{MFB} in each case were less than ± 7 °C. The increase in T_{MFB} against each reference surfaces depends on the surface characteristics (Table. 5) (Fig. 4a and 4b). First, although *L* was approximately 10 μm in the case of MS_{Brass} and $MS_{SUS316L}$, the increase in T_{MFB} compared to each reference surfaces is related to the thermal conductivity of surface micro-structures; in general, the order of *k* is 10^2 for the brass and 10^1 W/(m-K) for SUS316L, respectively (Fig. 4a). In addition, the *L* and *D* of the surface micro-structures were quite different between MS_{Brass} and $MS_{SUS316L}$ (Fig. 3 and Table 4). This indicates that the surface micro-structure does not always play a role in triggering the liquid–solid contact, even though *L* is at the micrometer scale. This result is distinct to several classical researches about the T_{MFB} considering surface roughness; they have believed that the surface roughness always causes a liquid–solid contact in film boiling regardless of its specific condition (e.g., *L, D, and* $< k >$).

Second, the increase in T_{MFB} also depends on the micro-structure characteristics under same surface super-hydrophilicity (C.A.~0°). The effect of surface super-hydrophilicity in T_{MFB} regardless of surface micro-structures can be independently checked by the results between RS_{Brass} and NS_{CuO}. The T_{MFB} in $MNS_{Brass/CuO}$ (300 °C) and NS_{CuO} (300 °C) also suggest that the surface micro-

Table 5
Minimum film-boiling quench temperature for different quench spheres.

I.D.	Structure scale	Substrate material (sphere diameter)	T_{MFB}, [°C]
$RS_{SUS316L}$	–	SUS316L ($d_{sphere} = 10$ mm)	239 ± 3
RS_{Brass}	–	Brass ($d_{sphere} = 10$ and 15 mm)	252 ± 5
$MS_{SUS316L}$	Micro	SUS316L ($d_{sphere} = 10$ mm)	257 ± 7
MS_{Brass}	Micro	Brass ($d_{sphere} = 10$ and 15 mm)	247 ± 5
$MNS_{Brass/CuO}$	Micro/Nano	Brass ($d_{sphere} = 15$ mm)	300 ± 5
MS_{CuO}	Micro	Brass ($d_{sphere} = 15$ mm)	Beyond 600
NS_{CuO}	Nano	Brass ($d_{sphere} = 15$ mm)	300 ± 5
RS_{Zr}	–	Zr ($d_{sphere} = 15$ mm)	302 ± 6
MS_{ZrO2}	Micro	Zr ($d_{sphere} = 15$ mm)	375 ± 6

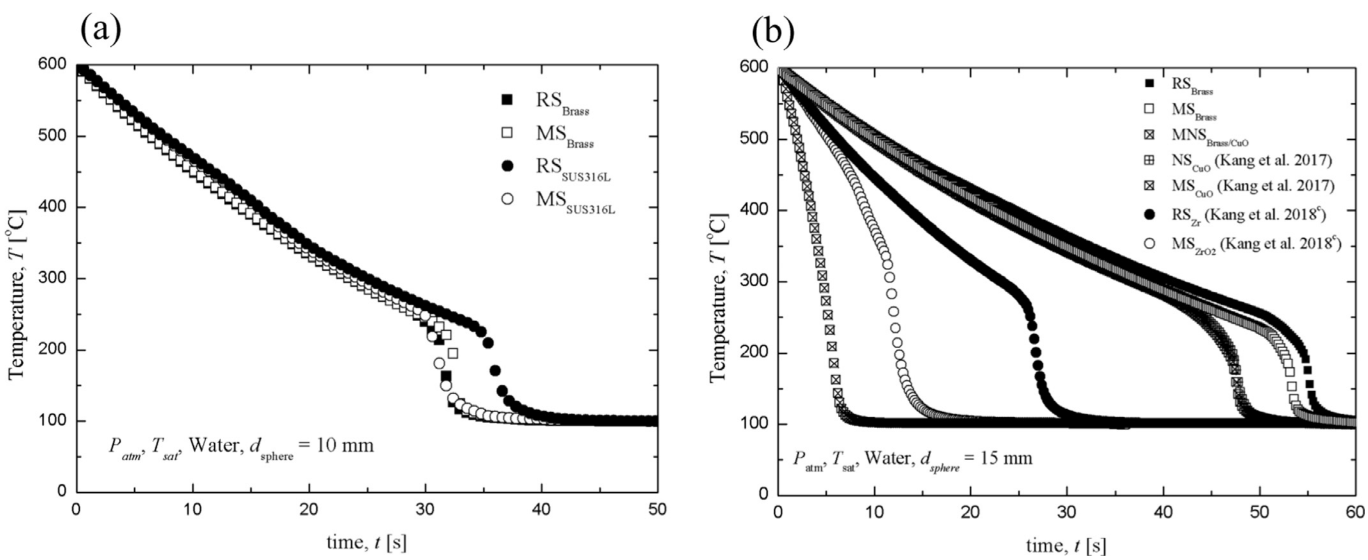

Fig. 4. Quench curve for the reference surface (RS) and micro-structured surface (MS): (a) $d_{sphere} = 10$ mm and (b) $d_{sphere} = 15$ mm.

structures ($L \sim 10\,\mu$m) with brass material ($k \sim 10^2$ W/(m-K)) does not play a role in the T_{MFB} increase (Fig. 4b).

Last, previous results of T_{MFB} we reported show that increases in T_{MFB} on MS_{CuO} and MS_{ZrO2} are represented by the characteristics of surface micro-structures under surface super-hydrophilicity (Fig. 4b) (Kang et al., 2017). Low $\langle k \rangle$ of surface micro-structures causes significant increase in T_{MFB}, and increased ratio in T_{MFB} compared to each reference (RS_{brass} and RS_{Zr}) depends on the L, D and $\langle k \rangle$, where $\langle k \rangle = \varphi k_v + (1-\varphi)k_s$ with local porosity $\varphi = 0.5$, vapor thermal conductivity k_v (~0.025 W/(m-K)) and solid thermal conductivity k_s (~1 W/(m-K) for CuO or ZrO_2), respectively (Samsonov, 2013).

Through this, we evaluated experimentally that change of characteristics in surface micro-structures determines the degree of T_{MFB} increase during quenching (Table. 5). This phenomenon is closely related to liquid–solid contact in film boiling, and seems to be explained by local cool-down of the micros-structure's tip, allowing the liquid to exist on the solid surface.

5. Discussions

5.1. Evaluation of T_{MFB}

Prior to evaluating the T_{MFB} increase, we checked the effect of sphere diameter on T_{MFB}. We use quench spheres with two diameters ($d_{sphere} = 10$ mm and 15 mm) and this belongs to the range of a small sphere (Hendricks and Baumeister, 1969). This criteria is based on the critical wavelength $\lambda_{cr} = 2\pi\lambda$ related to release of vapor bubble, where λ is the capillary length, $(\sigma_{lv}/\rho g)^{1/2}$ (De genes et al., 2013). When d_{sphere} is smaller than λ_{cr}, vapor bubble with a single dome forms in the film boiling from submerged quench sphere, and a multi-vapor dome is generated when d_{sphere} is larger than λ_{cr}. With λ_{cr} ~17 mm for saturation temperature of water at 1 atm, the vapor releasing dynamics on quench spheres we dealt with ($d_{sphere} < \lambda_{cr}$) is a vapor bubble with single dome.

By considering that the hydrodynamics of the liquid-vapor interface can influence T_{MFB}, we can check the liquid–vapor interfacial dynamics in film boiling during quenching through high speed visualization (Fig. 5). These results indicate that all of the quenching sphere exhibited single vapor bubbles. Therefore, the size effect of small quenching spheres is negligible in the T_{MFB} determination, which is within the range of 10 to 15 mm. This is also able to be proved by classical prediction in T_{MFB} suggested by Gunnerson and Cronenberg (1980); T_{MFB} for water weakly depends on d_{sphere} (the stainless steel sphere of diameters 6 and 9 mm, which are smaller than the λ_{cr}).

The surface micro-structures lead to a T_{MFB} increase in a water quenching experiment, and, this cannot be predicted by classical model in T_{MFB}. In particular, the predictive model considering the thermal effusivity $(\rho C_p k)^{1/2}$ of the surface did not predict T_{MFB} accurately for each reference surface (Table. 6), and this discrepancy was recently reported by Lee and Kim (2017), where ρ, C_p, and k are the density, specific heat of volume, and thermal conductivity, respectively. For example, all reference surfaces were treated by the annealing process before the quenching to match the same condition with the each micro-structured surface, and this probably impacts the T_{MFB} result in this experiment. In addition, we expected that T_{MFB} in each reference surfaces shows a reasonable result to evaluate the role of surface micro-structures, by comparing with a number of previous quench studies using a small sphere

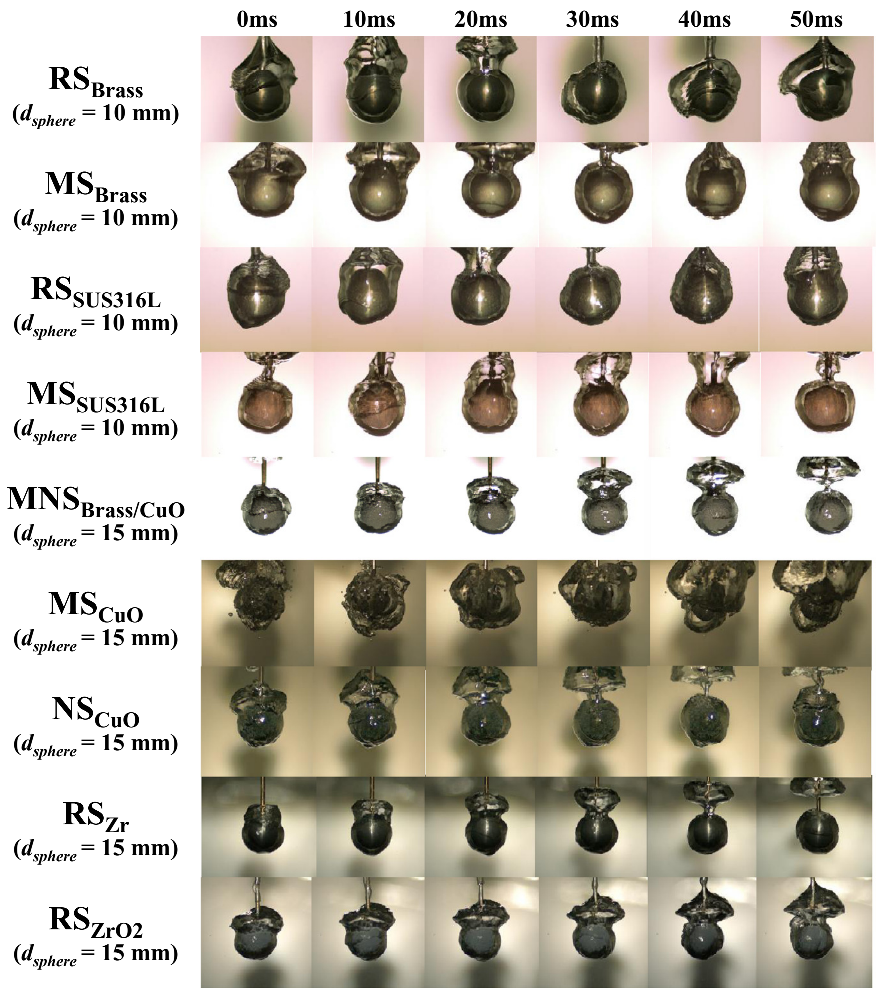

Fig. 5. High speed visualization images in film boiling on small spheres: T ~500 °C.

Table 6
Comparison evaluation of minimum film-boiling quench temperature T_{MFB} under saturation temperature water, 1 atm and reference surface condition.

Reference	Description	Specific condition	T_{MFB}, [°C]
Berenson (1961)	Prediction model	Consideration of hydrodynamics, infinite flat plate	186
Spiegler et al. (1963)	Prediction model	Consideration of thermodynamic limit	272
Henry (1974)	Prediction model	Consideration for thermal properties of heat transfer surface: Brass	290
Henry (1974)	Prediction model	Consideration for thermal properties of heat transfer surface: SUS316L	325
Henry (1974)	Prediction model	Consideration for thermal properties of heat transfer surface: Zr-702	439
Baumeister and Simon (1973)	Prediction model	Consideration for thermal properties of heat transfer surface: Brass	272
Baumeister and Simon (1973)	Prediction model	Consideration for thermal properties of heat transfer surface: SUS316L	272
Baumeister and Simon (1973)	Prediction model	Consideration for thermal properties of heat transfer surface: Zr-702	272
Kim et al. (2009)	Experiment	Quench, water, d_{sphere} = 9.5 mm, Stainless steel substrate, reference surface condition	250
Kim et al. (2009)	Experiment	Quench, water, d_{sphere} = 10 mm, Zircaloy substrate, reference surface condition	275
Xue et al. (2007)	Experiment	Quench, water, d_{sphere} = 50 mm, Nickel-plated copper substrate, reference surface condition	225
Zhang et al. (2013)	Experiment	Quench, water, d_{sphere} = 50 mm, Nickel-plated copper substrate, reference surface condition	225
Vakarelski et al. (2012)	Experiment	Quench, water, d_{sphere} = 20 mm, Steel substrate, reference surface condition	250
Fan et al. (2014)	Experiment	Quench, water, d_{sphere} = 10 mm, Stainless steel 304 substrate, reference surface condition	234
Fan et al. (2016)	Experiment	Quench, water, d_{sphere} = 10 mm, Stainless steel 304 substrate, reference surface condition	274
Present	Experiment	Quench, water, d_{sphere} = 10 mm, Stainless steel 316 substrate, reference surface condition	239
Present	Experiment	Quench, water, d_{sphere} = 10 mm, Nickel-plated brass substrate, reference surface condition	252
Present	Experiment	Quench, water, d_{sphere} = 15 mm, Nickel-plated brass substrate, reference surface condition	252
Present	Experiment	Quench, water, d_{sphere} = 15 mm, Zr-702 substrate, reference surface condition	302

Note: Atomic number n_0 at T_{MFB} calculation (Baumeister and Simon 1973) is assumed to be 29 for the Brass, 26 for the SUS316L, and 40 for the Zr-702, respectively.

with reference surface condition (Kim et al., 2009; Xue et al., 2007; Zhang et al., 2013; Vakarelski et al., 2012; Fan et al., 2014,2016).

Depending on the characteristics of surface micro-structures, the ratio of T_{MFB} increase compared to the reference surface is significantly different when the surface wettability is nearly identical. We reported the extreme increase in T_{MFB} on MS_{CuO} and explained this mechanism by the fin theory to describe the local tip-cooling in the micro-structure, causing the liquid–solid contact (Kang et al., 2017). It is well known that T_w to maintain the liquid–solid contact in film boiling should be lower than the homogeneous nucleation temperature, T_{hn}, of water (~330 °C), because the liquid phase above T_{hn} approaches the superheat limit of the liquid. It

Table 7
Thermal properties of test materials.

Material	Density, ρ [kg/m^3]	Specific heat of volume, C_p [J/(kg-K)]	Thermal conductivity, k [W/(m-K)]	Thermal diffusivity, α [m^2/s]
Brass	8500	380	121	0.000037
SUS316L	7990	500	21.4	0.000005
CuO	6400	531	1.0	0.00000029
Zirconium	6520	270	22.6	0.000013
ZrO_2	5700	502	1.7	0.000001

Note: The thermal properties are the value under $T = 25$ °C and 1 atm (Cengel, 2003;Samsonov, 2013;Bergman et al., 2011).

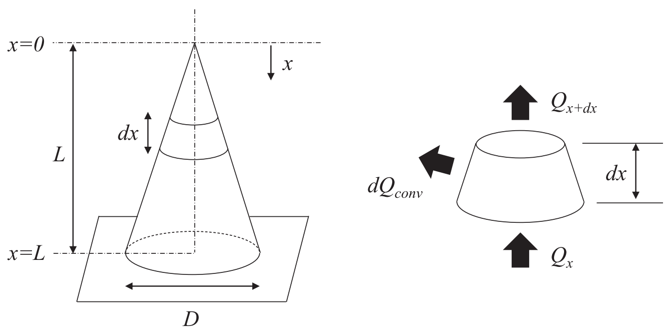

Fig. 6. Fin analysis of conical-spine fin geometry.

implies that the liquid can make contact with the quench surface if there is some local cold-spot that is close to T_{hn}. Therefore, close evaluation about the temperature profile of the surface micro-structures is necessary using the fin theory to determine the possibility of liquid–solid contact (Fig. 6).

5.2. Fin theory

A fin, or *extended* heat transfer surface, is an appropriate way to analyze the liquid–solid contact, because it is easy to evaluate control variables, such as the shape of the micro-structure, $<k>$, L, and D, considering the heat transfer; a number of studies have covered a variety aspects of a fin such as complicated geometries (Gardner, 1945) or ambient conditions (Han and Lefkowitz, 1960).

Fins have been widely used to improve the heat transfer by increasing the surface area. Whereas a high-efficiency fin is necessary to achieve its general purpose with a small temperature gradient, dT/dx, a low-efficiency fin will contribute to a large dT/dx, which causes liquid–solid contact. We evaluated the temperature profile of several surface micro-structures, which is modeled as micro-scale conical-spine fin under the film boiling condition, h $\sim 10^2$ W/(m^2-K).

The *Fourier number* $Fo = \alpha t/(L_c^2)$, of the surface micro-structures is relatively high (beyond unity) and it facilitates our fin analysis as quasi-steady-state problem, where α, and t is the thermal diffusivity ($k/\rho C_p$), and time, respectively. Thermal properties of each micro-structure were summarized in Table 7. The time is assumed to be contact duration, $t_c = 10$ ms (Lee et al., 1982, 1985; Kikuchi et al., 1992) and the characteristic length is the height of surface micro-structures L. For example, with $t_c = 10$ ms and $L = 10$ µm, Fo is about 3×10^3 for Brass ($\alpha = 3.7 \times 10^{-5}$), 5×10^2 for SUS316L ($\alpha = 5.0 \times 10^{-6}$), 6×10^1 for ZrO_2 ($\alpha = 1.0 \times 10^{-6}$), and 3×10^1 for CuO ($\alpha = 3.0 \times 10^{-7}$) respectively. Our fin analysis is based on *Murray-Gardner assumption* (Kraus et al., 2002) and detail derivation of the temperature gradient of surface micro-structures is available in *Appendix: fin theory*.

The dimensionless temperature difference of fin, $\theta^* = (T_{(x)} - T_{amb})/(T_{(x=L)} - T_{amb})$ and the fin efficiency η for conical-spine fin are

$$\theta^* = \left(T_{(x)} - T_{amb}\right)/\left(T_{(x=L)} - T_{amb}\right)$$

$$= \left(\frac{L}{x}\right)^{0.5} I_1\left[4(Bi_h)^{0.5}\left(\frac{x}{L}\right)^{0.5}\right]/I_1\left[4(Bi_h)^{0.5}\right] \tag{11}$$

$$\text{and, } \eta = \left[\frac{1}{(Bi_h)^{0.5}}\right] I_2\left[4(Bi_h)^{0.5}\right] I_1\left[4(Bi_h)^{0.5}\right], \tag{12}$$

where Bi_h, $T(x)$, T_{amb}, $T_{(x=L)}$, I_1, and I_2 are the *hybrid Biot number*, $hL^2/(<k>D)$, temperature, ambient temperature, fin base ($x = L$) temperature, *the modified Bessel function of the first kind of order one*, and *modified Bessel function of the first kind of order two*, respectively (Eqs. (A11), (A12), and (A17) of *Appendix*). The Bi_h is the thermal resistance ratio of fin conduction and surface convection (Lienhard, 2013), in analogy to the *modified Biot number*, $Bi_m = hL/k$ (Bradfield, 1966) first suggesting the physical parameters affecting the liquid–solid contact in stable film boiling.

The θ^* and η are divided by certain range in Bi_h (Fig 7a), where x is the axial length (Eqs. (A11) and (A17) of *Appendix*). In the first region (Bi_h $\langle 10^{-3}$), there was no temperature difference between the fin tip ($x = 0$) and fin base ($x = L$). The fin efficiency is unity in this region. In the second region (Bi_h: 10^{-3} $\sim 10^2$), the temperature difference begins to increase as the Bi_h increases. In the final region (Bi_h $\rangle 10^2$), the fin tip temperature $T_{(x=0)}$ equals T_{amb} as it would be in the case of an infinitely long fin. This indicates that even though the fin efficiency becomes relatively small (below 0.1), the fin tip temperature influencing the liquid–solid contact becomes the lowest.

We calculated temperature profile of the conical-spine micro-scale fin to evaluate the possibility of the liquid–solid contact during film boiling (Fig. 7b). We selected three cases of $\langle k\rangle$ to evaluate a wide range of Bi_h: $\langle k\rangle$ ~ 1 W/(m·K) for ZrO_2, $\langle k\rangle$ ~ 10 for SUS316L and $<k>\sim 100$ W/(m·K) for brass (Samsonov, 2013; Bergman et al., 2011). The fin base temperature $T_{(x=L)}$ was 600 °C, and T_{amb} was assumed to be the same as the film temperature $T_{film} = (T_{(x=L)} + T_{sat})/2$. The heat transfer coefficient h is assumed to be 250 W/(m^2-K) with vapor film thickness $\delta_v = 100$ µm and $k_v = 0.025$ W/(m-K), which is general order of film boiling heat transfer and its approximation, $h\delta_v/k_v = 1$ (Dhir and Purohit, 1978). The L^2/D is simplified as 100 with $L = 10$ µm and $D = 1$ µm.

In the case of $\langle k\rangle$ ~ 100 W/(m·K) (or, Bi_h $\sim 5 \times 10^{-4}$), there was no decrease in fin tip temperature during film boiling. This indicates that the micro-structures of the MS_{Brass} cannot cause local temperature drop, causing liquid–solid contact, and does not contribute to increases in T_{MFB} during quenching (Bi_h $\sim 3 \times 10^{-4}$ for MS_{Brass}). As $\langle k\rangle$ decreases, the fin tip temperature decreases when Bi_h is beyond 1×10^{-3} (Bi_h $\sim 3 \times 10^{-3}$ for $MS_{SUS316L}$). That is, micro-structures with low k can promote liquid–solid contact during film boiling due to local cooling of the microstructures, resulting in an increase in T_{MFB}. This is identical to our recent report about the fast quench on MS_{CuO}, causing increase in T_{MFB} beyond 600 °C (Kang et al., 2017).

5.3. T_{MFB} on micro-structured surfaces

Based on the fin analysis, we suggest a model for T_{MFB} on a micro-structured surface of a small sphere. Using the thermal re-

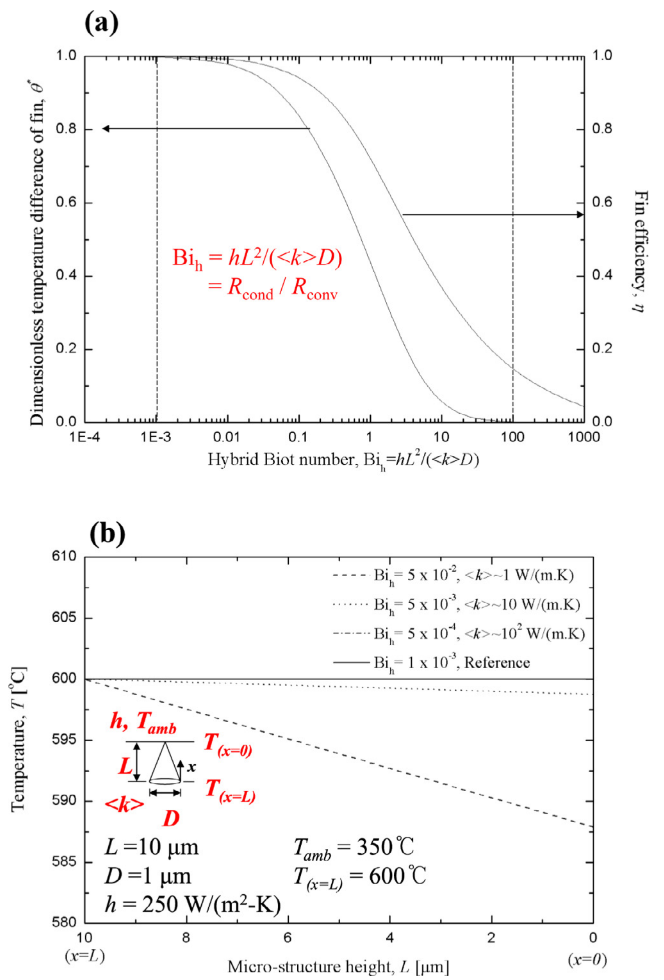

Fig. 7. (a) Fin-efficiency η and dimensionless temperature difference of fin θ^* versus *hybrid Biot number* Bi_h, and (b) temperature profile of micro-structures depending on Bi_h.

sistance analysis of the fin $R_{fin} = (T_{(x=L)} - T_{amb})/Q_{cond,(x=L)}$, T_{MFB} on micro-structured surface can be described;

$$Q_{cond(x=L)} = \left(T_{(x=L)} - T_{amb}\right)\left(\frac{\pi k^{0.5} h^{0.5} D^{1.5}}{2}\right) I_2 \times \left[4(Bi_h)^{0.5}\right] / I_1\left[4(Bi_h)^{0.5}\right], \tag{13}$$

$$R_{fin} = 1/(\eta A_s h), \tag{14}$$

$$\begin{aligned}\Delta T_{fin} &= Q_{cond(x=L)} R_{fin}(1-\theta^{**}) = \left(T_{(x=L)} - T_{amb}\right)(1-\theta^{**}) \\ &= T_{(x=L)} - T_{(x=0)} \\ &= \left(T_{((x=L))} - T_{amb}\right)\left\{1 - 2(Bi_h)^{0.5}/I_1\left[4(Bi_h)^{0.5}\right]\right\}, \text{ and}\end{aligned} \tag{15}$$

$$T_{MFB,MS} = T_{MFB,RS} + c\Delta T_{fin}, \tag{16}$$

where $Q_{cond,(x=L)}$, A_s, R_{fin}, ΔT_{fin}, θ^{**}, $T_{MFB,MS}$, $T_{MFB,RS}$, and c are the conduction heat from the fin base, surface area of fin, thermal resistance of fin, apparent temperature difference between fin tip and fin base, $T_{(x=L)}$-$T_{(x=0)}$, the dimensionless temperature between fin tip and fin base, $(T_{(x=0)}$-$T_{amb})/(T_{(x=L)}$-$T_{amb})$, minimum film-boiling quench temperature on micro-structured surface, minimum film-boiling quench temperature on reference surface, and weighting factor, respectively (from Eqs. (A14) to (A19) at *Appendix*).

The $T_{MFB}{}^*$ indicates the ratio between $T_{MFB,MS}$ and $T_{MFB,RS}$ and is calculated on the basis of the absolute temperature, which is a function of Bi_h, and is divided by three regions (Fig. 8). In the region of low Bi_h (below 10^{-3}), the micro-structure does not cause the liquid–solid contact during film boiling. An increase in T_{MFB} is determined by ΔT_{fin} in the intermediate region (Bi_h: 10^{-3} ~10^2), and is limited in the last region (beyond 10^2). This limitation is caused by the approximation of T_{amb} to T_{film}. We expect that although it is hard to fabricate micro-structures with a high Bi_h (for instance, $Bi_h = 10$, which corresponds to $L = 1$ mm, $D = 10$ µm, $\langle k\rangle = 1$ W/(m·K), $h = 250$ W/(m²·K), and $c = 3$), T_{MFB} can be maximized to approximately 1,000 °C under water quenching (1 atm and T_{sat}).

We also calculated the ratio between vapor film thickness and height of the surface micro-structures δ_v/L versus Bi_h, which is strongly related to the liquid–solid contact (Bradfield, 1966) (Fig. 8). We assumed that h, $\langle k\rangle$ *and* D is constant as 250 W/(m²-K), 0.5 W/(m²-K), and 1 µm, respectively. The heat transfer coefficient is assumed by the relation $h\delta_v\ / <k> = 1$ with $k_v = 0.025$ W(m-K), corresponding to δ_v with 100 µ suggested by Dhir and Purohit (1978). The Bi_h beyond 5 results in large δ_v/L (beyond 1). When Bi_h is below 5, the mechanism of the liquid–solid contact becomes through the local temperature drop, as opposed to destabilizing the liquid-vapor interface by *hydrodynamic instability*.

Our predicted values for T_{MFB} using the proposed model are in good agreement with previously reported (Kim et al., 2009) (Table. 8) (Fig. 8). For each micro-structured surface, the values for $T_{MFB,MS}$, $T_{MFB,RS}$, L, D, and h are provided for calculation of the ΔT_{fin} in Eq. (16) (Eq. (A19) of *Appendix*). The $T_{MFB,RS}$ in Eq. (16) indicates the reference surface condition obtained experimentally. Although surface micro-structures can exist on quenched surfaces, micro-structure with low Bi_h (i.e., $< k >$ ~500 W/(m·K) in the case of diamond) does not cause an increase in T_{MFB}. This contrasts with the T_{MFB} result of silica ($< k >$ ~0.5 W/(m·K)) and alumina ($< k >$ ~5 W/(m·K)) micro-structured surfaces under saturated water quenching.[1] The prediction model is in well agreement with our experimental results: MS_{Brass}, $MS_{SUS316L}$ and MS_{ZrO2} as well as high Bi_h case (MS_{CuO}) (Kang et al., 2017).

5.4. Approximation

The weighting factor c in Eq. (16) can be related to the following parameters: variable cross-section of fin, non-uniform heat transfer coefficient around fin $h(x)$, and the instantaneous superheat of liquid when liquid contacts to the heat transfer surface. Prior to a systematic study to identify the factor c, and we analyze an independent effect in the variable cross-section of fin, and the non-uniform heat transfer coefficient around fin $h(x)$, when the surface micro-structure is analyzed by fin theory.

5.4.1. Variable cross-section of fin

In the T_{MFB} correlation proposed in Section 5.3, we set a micro-structure as conical-spine fin geometry. Owing to surface polishing and surface corrosion, a non-uniform cross-section conical-spine Fig. 9a) is a more realistic approach than the uniform cross-section fin (e.g., cylindrical-spine geometry) (Eqs. (17), ((18)). The dimensionless temperature difference θ^* and efficiency η of the cylindrical-spine fin are (noting the relatively large conduction resistance $R_{cond} = L/(\langle k\rangle A)$ compared to the case of the conical-spine)

$$\theta^* = cosh\left[(2Bi_h)^{0.5}\,(x/L)\right]/cosh\left[(2Bi_h)^{0.5}\right], \text{ and} \tag{17}$$

[1] This micro-structured surface proposed by Kim et al. (2009) was prepared by the nano-particles deposition during boiling into nano-fluid. The nano-particles are aggregated and form the porous-micro-structures of which maximum height of surface roughness is about micrometer scale.

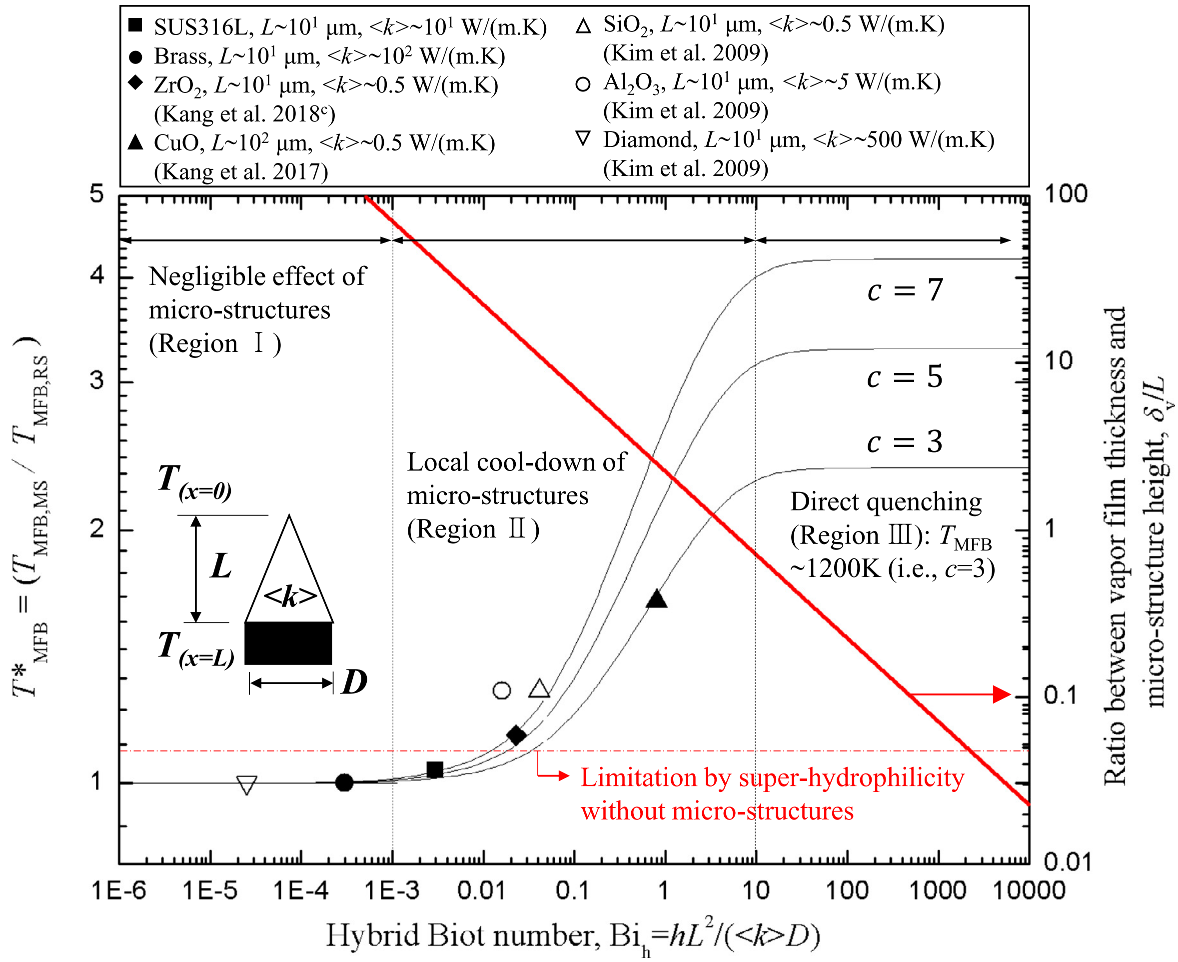

Fig. 8. T_{MFB} increase (or, $T_{MFB}{}^*$) and δ_v/L versus Bi_h.

Table 8
Hybrid Biot number of surface micro-structures under saturation film boiling condition.

I.D.	Fin height, L [µm]	Fin base diameter, D [µm]	Effective thermal conductivity of micro-structures, $\langle k \rangle$ [W/(m-K)]*	Heat transfer coefficient, h [W/(m2-K)]	*Hybrid Biot number,* $Bi_h = hL^2/(<k>D)$	$T_{MFB}{}^* = T_{MFB,MS}/T_{MFB,RS}$
$RS_{SUS316L}$	–	–	–	–	–	–
RS_{Brass}	–	–	–	–	–	–
$MS_{SUS316L}$	7	2	10	333	0.003	1.03
MS_{Brass}	10	25	100	333	0.0003	1.00
$MNS_{Brass/CuO}$	10	25	100	333	0.0003	1.08
MS_{CuO}	100	20	0.5	800	0.8	1.65
NS_{CuO}	–	–	–	–	–	1.08
RS_{Zr}	–	–	–	–	–	–
MS_{ZrO2}	10	5	0.5	585	0.023	1.12
Kim et al. (2009): SiO_2	12	5	0.5	727	0.041	1.24
Kim et al. (2009): Al_2O_3	21	5	5	900	0.016	1.29
Kim et al. (2009): Diamond	15	5	500	285	0.000025	1.00

Note: In case of the MS_{CuO}, MS_{ZrO2} and the experimental results from Kim et al. (2009), the vapor thermal conductivity k_v, and porosity φ is assumed to be 0.025 kW/m-K, and 0.5, respectively, when we calculate the effective thermal conductivity, $\langle k \rangle = \varphi k_v + (1-\varphi) k_s$. Also, thermal conductivity of solid k_s is assumed to be 1, 10, and 1000 for the SiO_2, Al2O3, and diamond, respectively.

$$\eta = \tanh\left[(2Bi_h)^{0.5}\right] / \left[(2Bi_h)^{0.5}\right]. \quad (18)$$

5.4.2. Non-uniform heat transfer coefficient around fin

An inherent characteristic of saturated film boiling is the wave motion of the liquid–vapor interface and this affects the local heat transfer rate, by changing the local vapor film thickness. The film boiling heat transfer is dominated by conduction and radiation, by neglecting radiation: $q" = \frac{k_v \Delta T_{sat}}{\delta_v(x)} = h(x)\Delta T_{sat}$ where ΔT_{sat} is the wall superheat, T_w-T_{sat}. From several literatures (Han and Lefkowitz, 1960; Chen and Zyskowski, 1963; Gardner, 1951), non-uniform heat transfer coefficient around fin can be described by $h(x) = (\gamma + 1)\ h((\frac{x}{L})^{\gamma}$, where γ is the distribution constant (Fig. 9b), with $\gamma =$ zero for the uniform, 1 for the linear distribution and 3 for the exponential distribution. The fin efficiency η, which indicates the ΔT_{fin}, decreases as the distribution constant

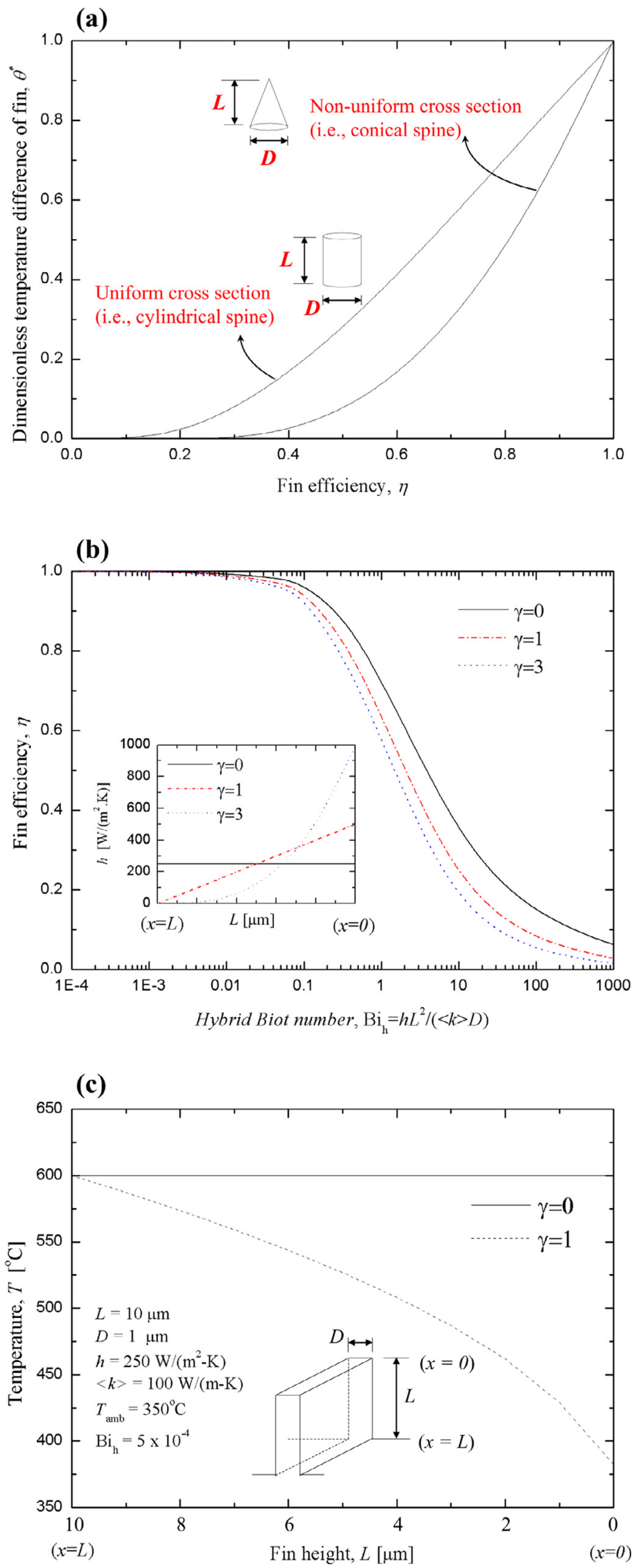

Fig. 9. Fin analysis of micro-structures: (a) fin-efficiency and dimensionless temperature difference of fin for different fin geometry, (b) effect of non-uniform heat transfer coefficient around the fin versus fin efficiency and *hybrid Biot number*, (c) temperature profile of micro-structures based on non-uniform heat transfer coefficient around fin.

increases. All cases show that the fin efficiency starts to decrease when Bi_h is beyond 10^{-3}.

We calculated the temperature gradient of micro-structures with different distributions of heat transfer coefficient (Fig. 9c). Fin geometry is selected using rectangular shape for simplification, and $T_{(x=0)}$ decreases as the γ increases. The effect of heat transfer distribution around fin will impact the fin tip cooling of micro-structures when the liquid-vapor interface of film boiling is wavy, and will be similar to variable cross-section area fin (an increase in the convection resistance, $R_{conv} = 1/(hA)$).

Even though we cannot completely quantify c, intuitively the fin tip temperature $T_{(x=0)}$ decreases as the Bi_h increases, causing the liquid–solid contact in film boiling. The trend of minimum film-boiling quench temperature increase $T^*_{MFB} = T_{MFB,MS}/T_{MFB,RS}$ remains valid regardless of c (strongly depends on Bi_h) (Fig. 8). The proposed model of T_{MFB} is based on a uniform heat transfer coefficient, i.e., more conservative.

6. Conclusion

The effect of surface micro-structures in T_{MFB} was investigated by a quench test (saturated water at 1 atm) with small-diameter spheres. The T_{MFB} increase by surface micro-structures is represented by *hybrid Biot number* $Bi_h = hL^2/(\langle k\rangle D)$, and this governs the local fin tip cooling, causing a liquid–solid contact.

Low $\langle k\rangle$ and high L^2/D of the surface micro-structure lead to a significant increase in T_{MFB} during quenching. Surface micro-structures of a small Bi_h below 10^{-3} cannot play a major role in triggering the liquid–solid contact, and thus, the increase in T_{MFB} is negligible. In particular, surface micro-structures of which Bi_h is beyond 10^2 is proposed for a maximum increase in the T_{MFB} under saturation temperature and atmospheric pressure of water condition.

Based on these results, we can design the heat transfer surface that delays the post-critical heat flux(CHF) regime under high-temperature conditions, by adding surface micro-structures with high Bi_h condition (beyond 10^2). Even though it will be further necessary to consider factors affecting T_{MFB} during quenching, such as the effect in a variable cross-section fin and non-uniform heat transfer coefficient around fin, we expect that this approach for predicting T_{MFB} by surface micro-structures contributes to a guideline in the development of advanced high-temperature cooling systems.

Acknowledgment

This work was supported by a National Research Foundation of South Korea (NRF) grant funded by the Korea government (MSIP) (NRF-2015M2A8A2074795). Also, M.K. is grateful for the support by U.S. NSF (Thermal Transport and Processes, CBET16235720).

Appendix. fin theory

All demonstrations in fin analysis are referred to textbook edited by Kraus (2002). Similar approach was already developed by our previous quench study: Kang et al., (2017).

The fin analysis is based on the energy balance equation Eq. (A1) with *Murray-Gardner assumption*;

(a) The heat flow in the fin and its temperature remain constant over time.
(b) The fin material is homogeneous; its thermal conductivity is the same in all directions, and it remains constant.
(c) The convective heat transfer coefficient on the face of the fin is constant and uniform over the entire surface of the fin.
(d) The temperature of the medium surrounding the fin is uniform.

(e) The fin thickness is small compared with its height and length; thus, the temperature gradient across the fin thickness and heat transfer from the edges of the fin may be neglected.
(f) The temperature at the base of the fin is uniform.
(g) There is no contact resistance where the base of the fin joins the prime surface.
(h) There are no heat sources within the fin itself.
(i) The heat transferred through the tip of the fin is negligible compared with the heat leaving its lateral surface.
(j) Heat transfer to or from the fin is proportional to the temperature excess between the fin and the surrounding medium.

$$Q_{cond,x} = Q_{cond,x+dx} + dQ_{conv}, \tag{A1}$$

$$Q_{cond,x} = -kA_{cs}(dT/dx), \tag{A2}$$

$$Q_{cond,x+dx} = Q_{cond,x} + \left(dQ_{cond,x}/dx\right)dx = -kA_{cs}(dT/dx) \\ -kd/dx(A_{cs}dT/dx)dx, \text{ and} \tag{A3}$$

$$dQ_{conv} = h(dA_s)(T - T_{amb}), \tag{A4}$$

where Q_{cond}, Q_{conv}, k, A_{cs}, T, x, h, A_s and T_{amb} are the conduction heat into fin, convection heat around fin, thermal conductivity, cross-section area of the fin, temperature, axial length, heat transfer coefficient around fin, surface area of the fin, and ambient temperature, respectively. By substituting each terms Eqs. (A2)–(A4) into Eq. (A1), the general form of the heat equation is obtained:

$$d^2T/dx^2 + (1/A_{cs})(dA_{cs}/dx)(dT/dx) \\ - (1/A_{cs})(h/k)(dA_s/dx)(T - T_{amb}) = 0. \tag{A5}$$

Contrast to constant A_{cs}, we consider A_{cs} as the function of x (e.g., conical-spine fin). The fin geometry is represented by the assumption of the surface profile $f_2(x)$;

$$f_2(x) = \left(\frac{D}{2}\right)\left(\frac{x}{L}\right)^{\frac{1-2n}{2-n}}, \tag{A6}$$

$$f_1(x) = \pi[f_2(x)]^2 = A_{cs}, \text{ and} \tag{A7}$$

$$f_3(x) = 2\pi f_2(x) = p, \tag{A8}$$

where n, D, L, and p is the geometric constant of the fin, fin base diameter, fin height, perimeter of the fin, respectively. For the conical-spine ($n = -1$), substitution of Eq. (A5) by Eqs. (A6)–(A8) results in the second order, homogeneous, ordinary differential equation,

$$[f_2(x)]^2\left(d^2\theta/dx^2\right) + d/dx[f_2(x)]^2 d\theta/dx - \left(\frac{2h}{k}\right)f_2(x)\theta = 0, \quad \text{or} \tag{A9}$$

$$x^2d^2\theta/dx^2 + 2xd\theta/dx - M^2x\theta = 0, \tag{A10}$$

where θ, M, and m are the temperature difference $T_{(x)}$-T_{amb}, $m(2\,L)^{1/2}$, and, $[2\,h/(kD)]^{1/2}$, respectively. Solution of Eqs. (A9) or (A10) is expressed by the general form of the *modified Bessel function of the first kind of order one* I_1, and, we can evaluate the temperature distribution along the fin, so called *dimensionless temperature of fin*, θ^*, as

$$\theta^* = \theta/\theta_{(x=L)} = \left(T_{(x)} - T_{amb}\right)/\left(T_{(x=L)} - T_{amb}\right) \\ = \left(\frac{L}{x}\right)^{0.5} I_1\left(2Mx^{0.5}\right)/I_1\left(2ML^{0.5}\right) \\ = \left(\frac{L}{x}\right)^{0.5} I_1\left[4(Bi_h)^{0.5}\left(\frac{x}{L}\right)^{0.5}\right]/I_1\left[4(Bi_h)^{0.5}\right], \tag{A11}$$

where $\theta_{(x=L)}$ and $\mathrm{Bi_h}$ is the temperature difference between fin base and ambient temperature $T_{(x=L)}$-T_{amb}, and *hybrid Biot number, $hL^2/(kD)$*, respectively. The solution in Eq. (A11) at singular point ($x = 0$) can be, in particular, obtained by *L'Hôpital's Theorem* by Eq. (A12):

$$\lim_{(x\to 0)} \theta_{(x=0)} = \lim_{(x\to 0)} \left[\frac{\theta_{(x=L)}\left(\frac{L}{x}\right)^{0.5} I_1\left(2Mx^{0.5}\right)}{I_1\left(2ML^{0.5}\right)}\right] \\ = \theta_{(x=L)}ML^{0.5}/I_1\left(2ML^{0.5}\right). \tag{A12}$$

Using Eq. (A12), we can theoretically express the *dimensionless temperature difference between fin tip and fin base, θ^{**}*;

$$\theta^{**} = \theta_{(x=0)}/\theta_{(x=L)} = \left(T_{(x=0)} - T_{amb}\right)/\left(T_{(x=L)} - T_{amb}\right) \\ = ML^{0.5}/I_1\left(2ML^{0.5}\right) = 2(Bi_h)^{0.5}/I_1\left[4(Bi_h)^{0.5}\right]. \tag{A13}$$

We need an apparent temperature difference between fin tip and fin base, $\Delta T_{fin} = T_{(x=L)} - \mathrm{T}_{(x=0)}$ to apply the prediction model in T_{MFB} on micro-structured surface such as relation: $T_{MFB,MS} \sim T_{MFB,RS} + c\Delta T_{fin}$ like Eq. (16) in manuscript, where $T_{\mathrm{MFB,MS}}$, $T_{\mathrm{MFB,RS}}$, and c are the minimum film-boiling quench temperature on micro-structured surface, minimum-film boiling quench temperature on reference surface, and weighting factor, respectively.

We analyze the thermal resistance of the fin $R_{fin} = \theta_{(x=L)}/Q_{cond,(x=L)}$. The heat transferred from the fin base, $Q_{cond,(x=L)}$ is calculated by the *Fourier's law* like Eq. (A2), by considering it as a function M through the *transformation of variable $u = 2M(x)^{1/2}$*:

$$Q_{cond,(x=L)} = kA_{cs}d\theta/dx_{(x=L)}, \text{ and} \tag{A14}$$

$$Q_{cond,(x=L)} = A_{cs}\left(2M^2/u\right)d\theta/du \\ = (\pi kD^2M\theta_{(x=L)}I_2\left(2ML^{0.5}\right)/\left[4L^{0.5}I_1\left(2ML^{0.5}\right)\right] \\ = \left(T_{(x=L)} - T_{amb}\right)\left(\pi k^{0.5}h^{0.5}D^{1.5}/2\right)\, I_2\left[4(Bi_h)^{0.5}\right]/I_1\left[4(Bi_h)^{0.5}\right], \tag{A15}$$

where I_2 is the *modified Bessel function of the first kind of order two*. The fin efficiency η is defined as the balance between $Q_{cond,(x=L)}$ and Q_{conv}. The Q_{conv} is ideal case of the heat transfer ($\eta = 1$), and, there is no spatial distribution of the temperature profile at the fin:

$$Q_{conv} = hA_s\theta_{(x=L)} = h\left[\left(\frac{\pi}{2}\right)DL\right]\theta_{(x=L)}, \quad \text{and} \tag{A16}$$

$$\eta = Q_{cond,(x=L)}/Q_{conv} = \left(2^{0.5}/mL\right)\left[I_2\left(2ML^{0.5}\right)/I_1\left(2ML^{0.5}\right)\right] \\ = \left[1/(Bi_h)^{0.5}\right]I_2\left[4(Bi_h)^{0.5}\right]/I_1\left[4(Bi_h)^{0.5}\right]. \tag{A17}$$

The fin resistance R_{fin} is represented in terms of the fin efficiency η, as follows:

$$R_{fin} = 1/(\eta A_s h). \tag{A18}$$

Using the Eqs. (A14)–(A18), we can summarize the ΔT_{fin} as a function of $\mathrm{Bi_h}$ like Eq. (A19):

$$\Delta T_{fin} = Q_{cond,(x=L)}R_{fin}(1 - \theta^{**}) = \theta_{(x=L)}(1 - \theta^{**}) = T_{(x=L)} - T_{(x=0)} \\ = \left(T_{(x=L)} - T_{amb}\right)\left\{1 - 2(Bi_h)^{0.5}/I_1\left[4(Bi_h)^{0.5}\right]\right\}. \tag{A19}$$

Our theory suggests that a fin theory elucidates the temperature distribution of surface micro-structures, and facilitates a development of prediction model of T_{MFB} on micro-structured surfaces taking into account the characteristics of the micro-structures (k, L, and D) as dimensionless number, so called *hybrid Biot number*, Bi_h. Final forms in minimum film-boiling quench temperature on micro-structured surface are proposed by $T_{MFB,MS} = T_{MFB,RS} + c\Delta T_{fin}$, or $(T_{MFB,\,MS}/T_{MFB,\,RS}) \sim c\Delta T_{fin}$.

References

Bang, I.C., Jeong, J.H., 2011. Nanotechnology for advanced nuclear thermal-hydraulics and safety: boiling and condensation. Nucl. Eng. Technol. 43 (3), 217–242.

Baumeister, K.J., Simon, F.F., 1973. Leidenfrost temperature—its correlation for liquid metals, cryogens, hydrocarbons, and water. J. Heat Transf. 95 (2), 166–173. doi:10.1115/1.3450019.

Berenson, P.J., 1961. Film-boiling heat transfer from a horizontal surface. J. Heat Transf. 83 (3), 351–356. doi:10.1115/1.3682280.

Bergman, T.L., Incropera, F.P., DeWitt, D.P., Lavine, A.S., 2011. Fundamentals of Heat and Mass Transfer. John Wiley & Sons.

Bernardin, J.D., Mudawar, I., 1999. The Leidenfrost point: experimental study and assessment of existing models. J. Heat Transf. 121 (4), 894–903. doi:10.1115/1.2826080.

Bradfield, W.S., 1966. Liquid–solid contact in stable film boiling. Ind. Eng. Chem. Fundam. 5 (2), 200–204. doi:10.1021/i160018a008.

Bromley, L.A., 1948. Heat transfer in stable film boiling. No. AECD-2295 (UCRL-122). Oak Ridge, Tenn., U.S. Atomic Energy Commission, Technical Information Division.

Carey, V.P., 1992. Liquid–vapor Phase-Change Phenomena. Taylor & Francis.

Cengel, Y.A., 2003. Heat Tranfer a Practical Approach. McGraw-Hill.

Chen, S.Y., Zyskowski, G.L., 1963. Steady state heat conduction in a straight fin with variable heat transfer coefficient. In: Proceedings of the Sixth National Heat Transfer Conference. New York, NY, USA. American Society of Mechanical Engineers, p. 1.

Chang, K.H., Witte, L.C., 1990. Liquid–solid contact in pool film boiling from a cylinder. J. Heat Transf. 112 (1), 263–266. doi:10.1115/1.2910359.

De Gennes, P.G., Brochard-Wyart, F., Quere, D., 2013. Capillarity and Wetting Phenomena: Drops, Bubbles, Pearls, Waves. Springer Science and Business Media.

Dhir, V.K., Purohit, G.P., 1978. Subcooled film-boiling heat transfer from spheres. Nucl. Eng. Des. 47 (1), 49–66. doi:10.1016/0029-5493(78)90004-3.

Dhuga, D.S., Winterton, R.H.S., 1985. Measurement of surface contact in transition boiling. Int. J. Heat Mass Transf. 28 (10), 1869–1880. doi:10.1016/0017-9310(85)90209-1.

Fan, Li-Wu, et al., 2014. Regulated transient pool boiling of water during quenching on nanostructured surfaces with modified wettability from superhydrophilic to superhydrophobic. Int. J. Heat Mass Transf. 76, 81–89. doi:10.1016/j.ijheatmasstransfer.2014.04.025.

Fan, Li-Wu, et al., 2016. Pool boiling heat transfer on a nanoscale roughness-enhanced superhydrophilic surface for accelerated quenching in water. Appl. Therm. Eng. 109, 630–639. doi:10.1016/j.applthermaleng.2016.08.131.

Gardner, K.A., 1945. Efficiency of extended surfaces. Trans. ASME 67 (1), 621–631.

Discussion on paper by Gardner, K.A., Ghai, M.L., 1951. Proc. General Discussion On Heat Transfer. Institute of Mechanical Engineers, London.

Gunnerson, F.S., Cronenberg, A.W., 1980. On the minimum film boiling conditions for spherical geometries. ASME J. Heat Transf. 102 (2), 335–341. doi:10.1115/1.3244284.

Han, L.S., Lefkowitz, S.G., 1960. Constant cross section fin efficiencies for non-uniform surface heat transfer coefficients. ASME Pap. 60.

Hendricks, R.C., Baumeister, K.J., 1969. NASA Technical Reports Server Document No. NASA TN D-5124. Lewis Research Center.

Henry, R.E., 1974. A correlation for the minimum film boiling temperature, 70, pp. 81–90.

Iloeje, O.C., et al., 1975. An investigation of the collapse and surface rewet in film boiling in forced vertical flow. J. Heat Transf. 97 (2), 166–172. doi:10.1115/1.3450336.

Kang, J., Kim, S.H., Jo, H., Park, G., Ahn, H.S., Moriyama, K., Kim, M.H., Park, H.S., 2016. Film boiling heat transfer on a completely wettable surface with atmospheric saturated distilled water quenching. Int. J. Heat Mass Transf. 93, 67–74. doi:10.1016/j.ijheatmasstransfer.2015.09.049.

Kang, J., Lee, G.C., Kaviany, M., Park, H.S., Moriyama, K., Kim, M.H., 2017. Minimum film-boiling quench temperature increase by CuO porous-microstructure coating. Appl. Phys. Lett. 110 (4), 043903. doi:10.1063/1.4974923.

Kang, J.Y, Lee, G.C., Kim, M.H., Moriyama, K., Park, H.S., 2018a. Subcooled water quenching on a super-hydrophilic surface under atmospheric pressure. Int. J. Heat Mass Transf. 117, 538–547. doi:10.1016/j.ijheatmasstransfer.2017.09.006.

Kang, J.Y., Kim, T.K., Lee, G.C., Kim, M.H., Park, H.S., 2018b. Quenching of candidate materials for accident tolerant fuel-cladding in LWRs. Ann. Nucl. Energy 112, 794–807. doi:10.1016/j.anucene.2017.11.007.

Kang, J.Y., Kim, T.K., Lee, G.C., Park, H.S., Kim, M.H., 2018c. Minimum heat flux and minimum film-boiling temperature on a completely wettable surface: effect of the Bond number. Int. J. Heat Mass Transf. 120, 399–410. doi:10.1016/j.ijheatmasstransfer.2017.12.043.

Kikuchi, Y., Hori, T., Michiyoshi, I., 1985. Minimum film boiling temperature for cooldown of insulated metals in saturated liquid. Int. J. Heat Mass Transf. 28 (6), 1105–1114. doi:10.1016/0017-9310(85)90119-X.

Kikuchi, Y., Takeshi, E., Itaru, M., 1992. Measurement of liquid–solid contact in film boiling. Int. J. Heat Mass Transf. 35 (6), 1589–1594. doi:10.1016/0017-9310(92)90047-V.

Kim, H, DeWitt, G., McKrell, T., Buongiorno, J., Hu, L.W., 2009. On the quenching of steel and zircaloy spheres in water-based nanofluids with alumina, silica and diamond nanoparticles. Int. J. Multiph. Flow 35 (5), 427–438. doi:10.1016/j.ijmultiphaseflow.2009.02.004.

Kim, H., Truong, B., Buongiorno, J., Hu, L.W., 2011. On the effect of surface roughness height, wettability, and nanoporosity on Leidenfrost phenomena. Appl. Phys. Lett. 98 (8), 083121. doi:10.1063/1.3560060.

Kondo, S., Konishi, K., Isozaki, M., Imahori, S., Furutani, A., Brear, D.J., 1995. Experimental study on simulated molten jet-coolant interactions. Nucl. Eng. Des. 155 (1), 73–84. doi:10.1016/0029-5493(94)00870-5.

Kozlov, N, Keßler, O., 2016. Influencing on liquid quenching by surface structuring. Int. J. Therm. Sci. 101, 133–142. doi:10.1016/j.ijthermalsci.2015.10.025.

Kraus, A.D., Aziz, A., Welty, J., 2002. Extended Surface Heat Transfer. John Wiley & Sons.

Lee, L., Chen, J.C., Nelson, R.A., 1982. Surface probe for measurement of liquid contact in film and transition boiling on high-temperature surfaces. Rev. Sci. Instrum. 53 (9), 1472–1476. doi:10.1063/1.1137160.

Lee, L.Y.W., Chen, J.C., Nelson, R.A., 1985. Liquid–solid contact measurements using a surface thermocouple temperature probe in atmospheric pool boiling water. Int. J. Heat Mass Transf. 28 (8), 1415–1423. doi:10.1016/0017-9310(85)90244-3.

Lee, C, Kim, A., Kim, J., 2015. Electrochemically etched porous stainless steel for enhanced oil retention. Surf. Coat. Technol. 264, 127–131. doi:10.1016/j.surfcoat.2015.01.004.

Lee, C.Y., In, W.K., Koo, Y.H., 2016. Transient pool boiling heat transfer during rapid cooling under saturated water condition. J. Nucl. Sci. Technol. 53 (3), 371–379. doi:10.1080/00223131.2015.1045952.

Lee, C.Y., Kim, S., 2017. Parametric investigation on transient boiling heat transfer of metal rod cooled rapidly in water pool. Nucl. Eng. Des. 313, 118–128. doi:10.1016/j.nucengdes.2016.12.005.

Lienhard, J.H, 2013. A Heat Transfer Textbook. Courier Corporation.

Moreaux, F., Chevrier, J.C., Beck, G., 1975. Destabilization of film boiling by means of a thermal resistance. Int. J. Multiph. Flow 2 (2), 183–190. doi:10.1016/0301-9322(75)90007-5.

Neti, S., Butrie, T.J., Chen, J.C., 1986. Fiber-optic liquid contact measurements in pool boiling. Rev. Sci. Instrum. 57 (12), 3043–3047. doi:10.1063/1.1138989.

Olek, S., Zvirin, Y., Elias, E., 1988. The relation between the rewetting temperature and the liquid–solid contact angle. Int. J. Heat Mass Transf. 31 (4), 898–902. doi:10.1016/0017-9310(88)90147-0.

Pan, L., Dong, H., Bi, P., 2010. Facile preparation of superhydrophobic copper surface by HNO 3 etching technique with the assistance of CTAB and ultrasonication. Appl. Surf. Sci. 257 (5), 1707–1711. doi:10.1016/j.apsusc.2010.09.001.

Sakurai, A., Shiotsu, M., Hata, K., 1990. Effects of system pressure on minimum film boiling temperature for various liquids. Exp. Therm. Fluid Sci. 3 (4), 450–457. doi:10.1016/0894-1777(90)90043-7.

Samsonov, G.V., 2013. The Oxide Handbook. Springer Science & Business Media.

Segev, A., Bankoff, S.G., 1980. The role of adsorption in determining the minimum film boiling temperature. Int. J. Heat Mass Transf. 23 (5), 637–642. doi:10.1016/0017-9310(80)90007-1.

Shoji, M., Witte, L.C., Sankaran, S., 1990. The influence of surface conditions and subcooling on film-transition boiling. Exp. Thermal Fluid Sci. 3 (3), 280–290. doi:10.1016/0894-1777(90)90003-P.

Sinha, J, 2003. Effects of surface roughness, oxidation level, and liquid subcooling on the minimum film boiling temperatu. Exp. Heat Transf. 16 (1), 45–60. doi:10.1080/08916150390126478.

Spiegler, P., Hopenfeld, J., Silberberg, M., Bumpus, C.F., Norman, A., 1963. Onset of stable film boiling and the foam limit. Int. J. Heat Mass Transf. 6 (11), 987–989. doi:10.1016/0017-9310(63)90053-X.

Tian, F., Hu, A., Li, M., Mao, D., 2012. Superhydrophobic nickel films fabricated by electro and electroless deposition. Appl. Surf. Sci. 258 (8), 3643–3646. doi:10.1016/j.apsusc.2011.11.130.

Vakarelski, I.U., et al., 2012. Stabilization of Leidenfrost vapour layer by textured superhydrophobic surfaces. Nature 489 (7415), 274–277. doi:10.1038/nature11418.

Xiao, X., et al., 2011. A facile process to prepare copper oxide thin films as solar selective absorbers. Appl. Surf. Sci. 257 (24), 10729–10736. doi:10.1016/j.apsusc.2011.07.088.

Xue, H.S., Fan, J.R., Hong, R.H., Hu, Y.C., 2007. characteristic boiling curve of carbon nanotube nanofluid as determined by the transient calorimeter technique. Appl. Phys. Lett. 90 (18), 184107. doi:10.1063/1.2736653.

Yao, S.C., Henry, R.E., 1978. An investigation of the minimum film boiling temperature on horizontal surfaces. J. Heat Transf. 100 (2), 260–267. doi:10.1115/1.3450793.

Zhang, L., et al., 2013. Enhanced critical heat flux during quenching of extremely dilute aqueous colloidal suspensions with graphene oxide nanosheets. J. Heat Transf. 135 (5), 054502. doi:10.1115/1.4023304.